ACCOUNTS
of chemical research

Two-Dimensional Electronic Spectroscopy of Molecular Aggregates

NAOMI S. GINSBERG, YUAN-CHUNG CHENG,[‡] AND
GRAHAM R. FLEMING[*]

California Institute for Quantitative Biosciences and Department of Chemistry, University of California, Berkeley, and Physical Biosciences Division, Lawrence Berkeley National Laboratory, Berkeley, CA

CONSPECTUS

The properties of molecular aggregates, coupled clusters of small molecules, are often challenging to unravel because of their inherent complexity and disordered environments. Their structure−function relationships are often far from obvious. However, their ability to efficiently channel excitation energy over remarkable distances, as is the case in photosynthetic light harvesting, is a compelling motivation to investigate them. Understanding and subsequently mimicking the processes in photosynthesis, for example, will set the stage for considerable advances in using light harvesting to fuel renewable energy technologies.

Two-dimensional (2D) electronic spectroscopy is emerging as a nonlinear optical technique that provides significant insight into the interactions and dynamics of complex molecular systems. In addition to spectrally resolving excitation and emission energies over significant bandwidths with femtosecond resolution, this technique has already enabled discoveries about the structure and dynamics of photosynthetic light-harvesting complexes and other aggregates.

Multiple capabilities unique to 2D electronic spectroscopy enable such findings. For example, the spectral resolution of excitation and emission combined with the ability to eliminate the effects of static disorder can reveal the homogeneous line width of a transition and the different dynamic contributions to it. Two dimensional spectroscopy is also sensitive to electronic coherence and has been employed to identify and characterize coherent excitation energy transfer dynamics in photosynthetic systems and conjugated polymers.

The presence of cross-peaks, signals for which excitation and emission occur at different wavelengths, provides multiple forms of information. First, it allows the identification of states in congested spectra and reveals correlations between them. Second, we can track excitation energy flow from origin to terminus through multiple channels simultaneously. Finally, 2D electronic spectroscopy is uniquely sensitive to intermolecular electronic coupling through the sign and amplitude of the cross-peaks. This feature makes it possible to reveal spatial molecular configurations by probing electronic transitions. Another means of "resolving" these angstrom-scale arrangements is to manipulate the probing laser pulse polarizations. In this way, we can isolate and modulate specific processes in order to retrieve structural information.

In this Account, we demonstrate these capabilities through a close collaboration between experiments and modeling on isolated photosynthetic pigment−protein complexes and also on J-aggregates. Each of the probed systems we describe offers insights that have both increased the utility of 2D electronic spectroscopy and led to discoveries about the molecular aggregates' dynamics and underlying structure.
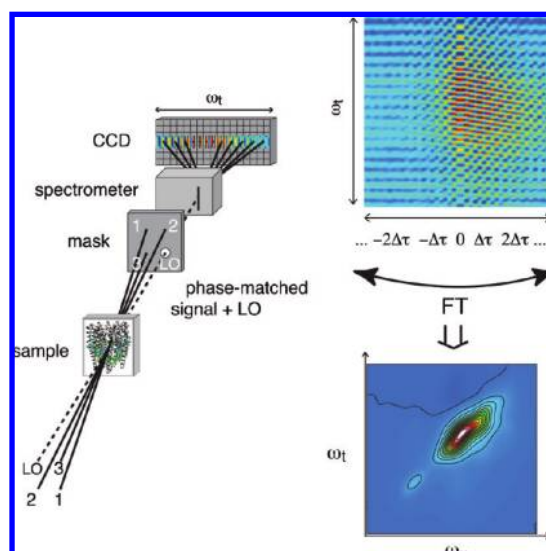
1. Introduction

Molecular aggregates are self-assembling clusters of small molecules with intermolecular separations typically close to individual molecule size. Coulomb interactions stabilize their configuration, determine their optical properties, and enable neutral electronic excitation energy to migrate through them. Some molecular aggregates reside in nature, such as in photosynthetic light harvesting.[1,2] Artificial counterparts[3−5] are increasingly being developed to achieve similarly efficient and rapid energy flow. Nevertheless, probing and modeling these complexes poses sizable challenges, because they present densely packed spatial and energetic landscapes and operate out of equilibrium in the condensed phase.[6−9]

By presenting a sample's optical response as a function of excitation and emission resonances, 2D electronic spectroscopy[10−13] measures how molecules within a complex interact with one another and volley electronic excitations. Despite several important distinctions, much of the formalism employed at optical frequencies was developed for 2D magnetic resonance experiments.[14] These efforts were first extended into the infrared to obtain ultrafast structural information by directly probing molecular vibrations[13,15,16] and are now being applied in the optical regime, addressing ultrafast electronic dynamics and structure. Here, stringent phase stability requirements and interferometric signal detection obstacles had to be surmounted.[17−19]

The aim of this Account is to provide an intuitive yet comprehensive understanding of 2D electronic spectroscopy and of the recent and rapid progress that has been made in applying it to photosensitive molecular aggregates. Diversity in both methods and discoveries is exhibited through a series of examples.

2. Principles of 2D Electronic Spectroscopy

In order to convey how and why 2D electronic spectroscopy is useful for studying molecular complexes, this section describes the ultrafast, nonlinear techniques used to obtain 2D spectra. We also describe how this information is interpreted in order to study electronically coupled molecular aggregates.

2.1. Measuring 2D Spectra. In a 2D electronic spectroscopy experiment, three laser pulses are used to stimulate the sample medium in order to measure its so-called third-order optical response. A 2D electronic spectrum is a plot of this response as a function of optical excitation and emission frequencies. Each point in the spectrum is the output signal of the ensemble of molecules resulting from its interaction with the three resonant electric fields.[20] The sample is illuminated with
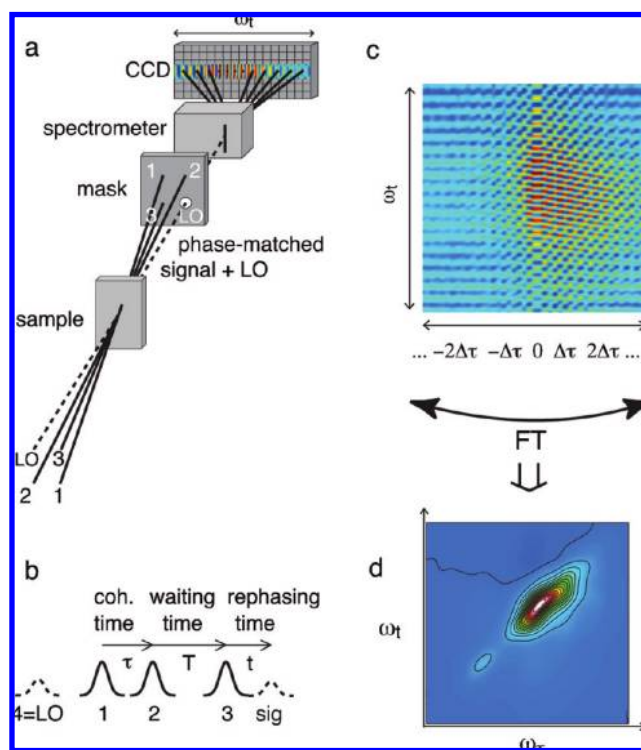

FIGURE 1. 2D spectra are constructed from the output signals of repeated three-pulse sequences. (a) Four light pulses impinge on a sample in a box geometry. Pulses 1, 2, and 3 generate the signal, which is heterodyne-detected with the weaker, copropagating local oscillator (LO). The signal and LO are dispersed at a grating onto a CCD. (b) Variable time delays between light pulses. The coherence time, τ, is swept from negative to positive values in order to generate a full 2D spectrum. Dynamics are observed during the waiting time T. The delay between pulse 3 and the output signal is referred to as the rephasing time. To assemble a 2D spectrum for a specific T, the detected signals for a set of coherence times spaced by $\Delta\tau$ are stacked (c) and are Fourier transformed (d).

three individual ultrafast laser pulses with controllable relative delays (Figure 1a). We denote the delay between pulses 1 and 2 by τ and the delay between pulses 2 and 3 by T. This pulse sequence (Figure 1b) results in the build-up of a macroscopic polarization in the medium that generates the signal of interest following pulse 3 after a delay, t. The noncollinear pulse geometry employed in this experiment ensures isolation of the signal in the $\vec{k}_{signal} = -\vec{k}_1 + \vec{k}_2 + \vec{k}_3$ wavevector phase-matching direction. To characterize the sample polarization in amplitude and phase, a fourth attenuated light pulse serves as a local oscillator (LO) to heterodyne-detect the emitted signal.[17] The signal and LO copropagate through a spectrometer, which disperses an interferogram onto a CCD camera. Hence the emission frequency of the signal corresponds to the pixel axis of the CCD (Figure 1b).

A complete 2D spectrum plots the detected electric field as a function of excitation and emission frequencies, ω_τ and ω_t, for a given waiting time, T: $E_s(\omega_\tau, T, \omega_t)$. The frequencies ω_τ and

ω_t are conjugate variables to τ and t, respectively (Figure 1b). Though the spectrometer measures the signal dependence on emission frequency ω_t, the dependence on excitation frequency ω_τ must be obtained by repeating the three-pulse sequence while varying the delay τ from negative to positive values. By literally "stacking" up these repeated measurements (Figure 1c) and Fourier transforming with respect to τ, one recovers the excitation frequencies, resulting in a 2D spectrum (Figure 1d). Repeating this process to obtain 2D spectra at different waiting times, T, enables direct measurement of dynamics.

Though the full, complex electric field of the signal is recorded, the absorptive rather than refractive medium response (real part only)[11,21] is presented in all spectra in this Account unless otherwise indicated. To isolate this absorptive portion, the complex-valued signal must have the correct phase factor, which is determined by fitting a projection of the 2D signal to corresponding spectrally resolved pump−probe data.[11,21]

2.2. Signal Contributions to 2D Spectra. The light pulse energies in 2D experiments are deliberately only strong enough to weakly perturb the system under study,[22] propagating small fractions of the complexes' wave functions either between ground and singly excited states or between singly and doubly excited states. Though, including the signal generation, there are four sequential light−matter interactions, a 2D spectrum is usually plotted as a function of the transition energies of the first and last. The first light pulse excites a superposition state, while the second and third further manipulate the aggregate electronic wave functions to induce coherent emission. The complete third-order signal detected in the phase-matched direction includes all possible energy- and momentum-conserving sequences of resonant interactions that link the aggregate electronic states. Many different such trajectories through the state space, or Liouville pathways,[20] occur simultaneously in the ensemble and can interfere with one another.

Generally speaking, system evolution occurs in electronic superposition states during both periods τ and t, the so-called coherence and rephasing times. In highly disordered condensed-phase systems, transition energies of individual molecules are altered by their local environments, inhomogeneously broadening the transition line widths. In this case, the phase evolution of different molecules' superposition states during τ and t varies throughout the ensemble. However, provided that transition energy-altering differences in local molecular environments do not vary over the time scale of the experiment, an important phenomenon occurs: when the density-matrix elements of a particular Liouville pathway have opposite phases of the same magnitude during τ and t, the total phase evolution for each aggregate involved independently sums to zero. Since the sample interacts with coherent laser light, the emergent light field is thus the result of constructive interference of the signals from many individual complexes that once again share the same relative phase. Thus, the coherent macroscopic signal, a photon echo, is immune to inhomogeneous broadening and allows the measurement of the homogeneous line width.[20]

2.3. Interpreting 2D Spectra. Interpreting 2D spectra requires understanding how various Liouville pathways manifest themselves in the signals. In this context, we discuss the most important characteristics of 2D spectra of electronically coupled systems: peak location, evolution, origin, and shape.

To illustrate the essential elements of a 2D spectrum, consider the fundamental constituent of a molecular aggregate, the coupled dimer of optically excitable molecules, or chromophores, in Figure 2a. This model provides intuition for the more complicated systems subsequently discussed. In the absence of Coulomb interaction, the molecules have respective ground and excited states, g_a, e_a and g_b, e_b. However, a coupling interaction J mixes their wave functions to form four new states delocalized over the two sites: a single ground state, two excited states e_1 and e_2, and a doubly excited state, f, corresponding to both molecules being excited simultaneously. Optical spectroscopy probes the transitions of this *excitonic* energy landscape,[1] illustrated in Figure 2b. The degree of excitonic coupling J depends on the proximity and relative orientation of the molecules.

These same parameters also determine the redistribution of transition strength among the excitons. For example, the configuration of the dipoles in Figure 2 leads to stronger absorption by e_1 and reduced absorption by e_2, manifested in multiple ways in the 2D spectrum. First, a cut along the diagonal of Figure 2c, where excitation and emission occur at the same energy, reflects the dimer's linear absorption. Second, off-diagonal contributions, or cross-peaks, exist at coordinates (e_1, e_2) and (e_2, e_1) and in this example have opposite sign. This underscores the importance of detecting the signal field rather than its intensity. These contributions indicate correlations between excitons and arise both due to electronic coupling between chromophores and due to nonradiative relaxation between excited states. The cross-peaks that develop due to population relaxation make 2D electronic spectroscopy ideal for visualizing energy transfer and are the focus of section 3.1.[23]
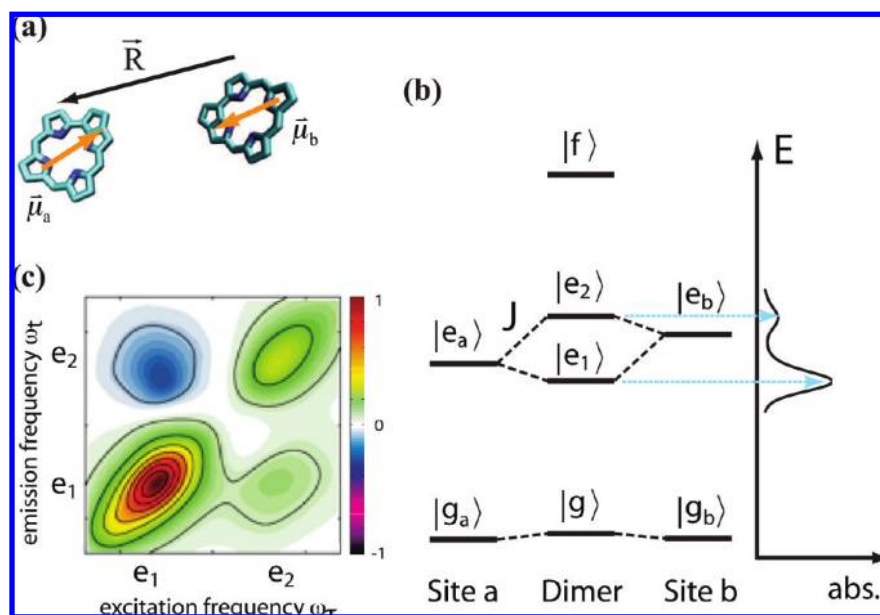
FIGURE 2. A coupled dimer of chlorophyll pigments: (a) chromophores are approximated as two-level electronic systems; (b) excitons e_1 and e_2 are superpositions of original states e_a and e_b, and are split due to coupling J, while f corresponds to two quanta of excitation. The coupling also redistributes transition strength, shown in the absorption spectrum at right and also in the dimer 2D spectrum at $T = 0$ (c).

Crosspeaks arising from electronic coupling are best visualized before population dynamics occur, at or near $T = 0$, as shown in Figure 2c. They originate from an imbalance in competing, colocated off-diagonal signal contributions of opposite sign. Liouville processes involving transitions between g and e_1 or e_2 only, for example, absorption and emission at e_1 followed by absorption and emission at e_2, contribute a positive signal due to the final emission from a single-exciton state. On the other hand, processes in which absorption and subsequent emission occur between the single-exciton states and f generate negative "excited state absorption" signals. Contributions from these two different types of pathways cancel, eliminating cross-peaks, if $J = 0$.[12] For $J \neq 0$, the dominant contribution determines the cross-peak's sign. Last, since the cross-peak sign depends on relative transition strengths, it is also an indicator of the relative orientation of the contributing molecular dipoles and can thus be used to determine the structure of molecular aggregates[24,25] (see section 3.5).

Finally, in addition to location and amplitude, peak shape provides dynamical information about the aggregate. Because of the effect of the photon echo, many features are narrower along the antidiagonal direction, where the inhomogeneous broadening is suppressed. Two dimensional electronic spectroscopy thus discerns various homogeneous and inhomogeneous line broadening mechanisms.

2.4. Rephasing and Nonrephasing Contributions to 2D Spectra. Further dissecting spectra according to pulse ordering clarifies the origin of features and distinguishes between different processes.[26–28] Recall that a complete 2D spectrum combines information obtained from repeated three-pulse sequences as the coherence time τ is varied. The *rephasing* photon echo signal pulse arises after finite rephasing time t from sequences when pulse 1 precedes pulse 2 ($\tau \geq 0$), provided the signal is recorded in the $-\vec{k}_1 + \vec{k}_2 + \vec{k}_3$ direction. As described in section 2.2, the ground−excited state superpositions during τ and t have opposite phases in a rephasing sequence. When the time ordering of pulses 1 and 2 is reversed ($\tau \leq 0$), the phase factors of superpositions during the coherence and rephasing times add rather than cancel, resulting in a *nonrephasing* signal immediately following the arrival of pulse 3 (free induction decay) that provides complementary information. By comparison with positively correlated rephasing line shapes, nonrephasing peaks have anticorrelated shapes, extending instead in the antidiagonal direction.[14,27]

Analyzing rephasing and nonrephasing signals separately[24,26] is particularly useful for interpreting 2D spectra. For example, the decay rate of the relative amplitude of rephasing and nonrephasing signals depends on the characteristic time scale over which the system's transition energies remain correlated with their former selves.[28,29] Separating rephasing and nonrephasing signals can also enable the assignment of peaks with greater certainty because any interference between their overlapping line shapes is eliminated. Furthermore, cross-peaks often are most easily distinguished in nonrephasing spectra since dominant diagonal peak pho-
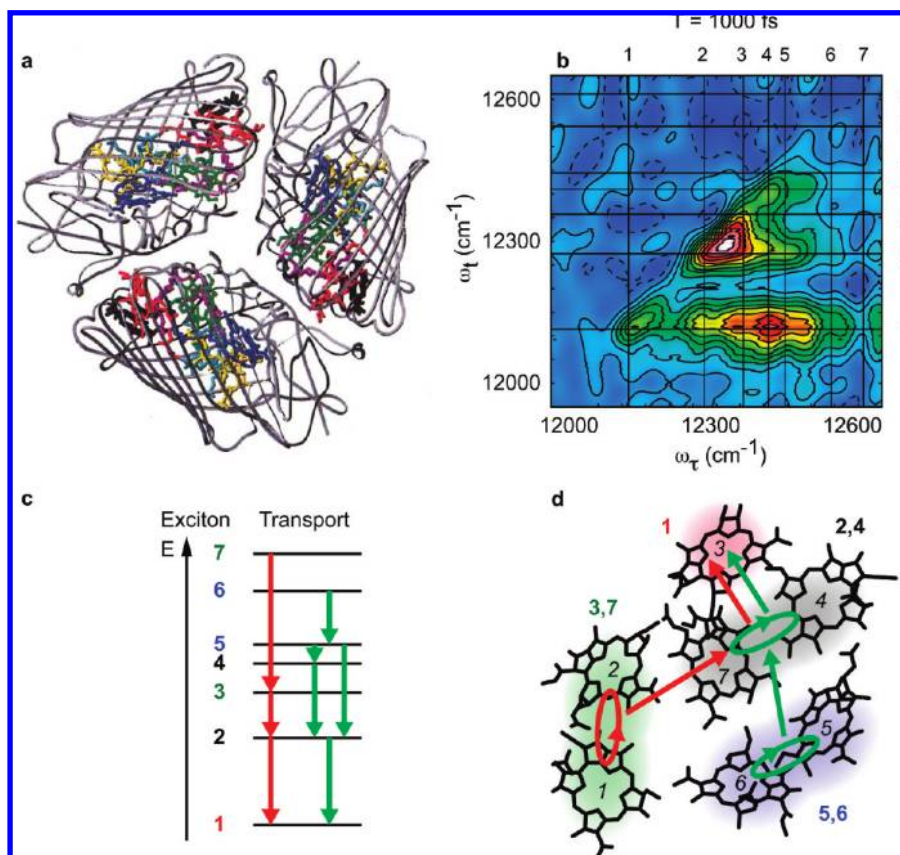
FIGURE 3. Two dimensional spectroscopy of FMO reveals energy transfer channels and explains why its structure efficiently promotes such transfer.[23] (a) FMO crystal structure (PDB ID 4BCL). Each of three monomers contains seven BChls. (b) $T = 1$ ps 2D spectrum of FMO complexes at 77 K with many clearly visible energy transfer peaks. Exciton energies are indicated on both axes. (c) Reconstruction of nonstepwise energy transfer channels based on 2D spectrum analysis. (d) Spatial map of energy flow from panel c in an FMO monomer.

ton echo signals are absent. We return to this point when discussing excited state coherence signatures[28,30] (section 3.4) and isolation of energy transfer cross-peaks for structure determination[24] (section 3.5.2).

3. What Do 2D Electronic Spectra of Molecular Aggregates Reveal?

Drawing on the preceding foundation, we now demonstrate how 2D electronic spectroscopy, combined with theoretical modeling, addresses many challenges and difficulties associated with characterizing the dynamics and electronic and structural properties of molecular aggregates in unprecedented ways.

3.1. Determining Parallel Excitation Energy Transfer Channels in FMO. In other optical spectroscopies such as transient absorption, it is difficult to directly determine the flow of excitation energy, both along the energy landscape and spatially. At best, one detects the net instantaneous amount of population in a given state or band. With 2D spectroscopy, cross-peaks often enable the resolution of states despite diagonal congestion, and one can determine the origin of excita-

tion energy arriving to a particular state. The ability to visualize states and the parallel excitation energy flow between them is exemplified in the 2D spectroscopy[23,31] of the Fenna−Matthews−Olson (FMO) photosynthetic pigment−protein complex from green sulfur bacteria, whose X-ray crystal structure is presented in Figure 3a. FMO links sacks of light-harvesting pigments to the membrane-bound reaction center that initiates the biochemistry of photosynthesis. This complex is a prototypical system for studying light harvesting and energy transfer in photosynthesis.[9,23,31,32] Energy transfer to the lowest exciton state of FMO from all six others is nearly complete by 1 ps.[32] Nevertheless, the particular trajectories of excitation energy flow across the bacteriochlorophyll (BChl) pigments had not been elucidated prior to the 2D spectroscopic study performed by Fleming and co-workers.[23,31]

Figure 3b displays the $T = 1$ ps 2D spectrum of FMO at 77 K. Multiple prominent cross-peaks below the diagonal, indicating parallel energy transfer channels, are distinguishable. For example, the strongest cross-peak at coordinates (ω_4, ω_1) indicates population transfer from exciton 4 to 1. By analysis of cross-peaks at multiple waiting times, a map of energy flow
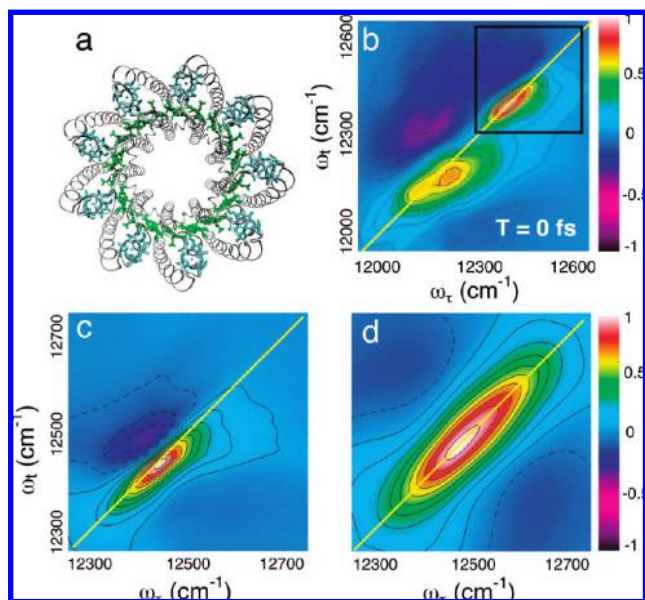
FIGURE 4. B800 coupling in LH3:[34] (a) LH3 crystal structure (PDB ID 1IJD) with symmetric, strongly coupled B820 ring of 18 BChls (green) and weakly coupled B800 ring of 9 BChls (cyan); (b) experimental 2D electronic spectrum of B820 and B800 bands of LH3 at 77 K, with the B800 region boxed; (c) calculated B800 2D spectrum for nearest-neighbor excitonic coupling $J = 30$ cm^{-1}; (d) calculated B800 2D spectrum for $J = 0$.

within FMO was constructed (Figure 3c). It reveals two main channels leading to the pooling of energy in the lowest exciton state, which is predominantly localized on pigment 3 positioned near the reaction center.[33] These findings were related to the spatial BChl configuration in a monomer (Figure 3d), where exciton wave functions in the model are distributed across at most two BChls. The facility of energy transfer between colocalized excitons, for example, between excitons 7 and 3 (green) both residing on pigments 1 and 2, explains how certain states are passed over during relaxation to the lowest state in the manifold.

3.2. Elucidating the Effects of Electronic Coupling in LH3. Unlike linear absorption and conventional pump−probe techniques, 2D electronic spectroscopy is highly sensitive to the degree of electronic coupling between chromophores. Zigmantas et al. studied light-harvesting complex 3 (LH3) from photosynthetic purple bacteria using 2D electronic spectroscopy.[34] LH3 contains nine identical subunits in a symmetric ring-like structure as shown in Figure 4a. The BChl pigments form two rings: a closely packed B820 ring (green) and a sparser B800 ring (cyan), each named after its absorption maximum. Relatively large separations between the B800 pigments have been used to justify neglecting the coupling between them.[6]

The experimental $T = 0$ 2D spectrum of LH3 at 77 K (Figure 4b) shows that both the B800 (boxed) and B820 bands

are highly asymmetric about the diagonal, indicative of electronic couplings within both rings. By analogy with the dimer spectrum in Figure 2, the 2D spectrum of the B800 band can be considered to arise from multiple coupled nearest-neighbor dimers whose excitons are not clearly resolved. Interference between the diagonal peak (positive) and the strong above-diagonal excited-state absorption cross-peak (negative) is responsible for the asymmetric band shape observed. In the case of the B800 ring, modeling shows that a small nearest-neighbor coupling of ~30 cm^{-1} (about 50% of k_BT at the 77 K temperature of the experiment) not only shifts transition strength to the lower excitons in the band but is also sufficient to reproduce the asymmetry[35] (Figure 4c). However, omitting the coupling results in perfect symmetry about the diagonal (Figure 4d) that does not agree with the experimental result. This study demonstrates the exquisite sensitivity of the 2D peak shape to weak couplings, even when cross-peaks are not resolved.

3.3. Discerning Broadening Mechanisms in J-aggregates. Line broadening can have many dynamic contributions between which it is often difficult to distinguish.[36] However, 2D spectroscopy can be more discerning than other spectroscopies, for example by resolving homogeneous line widths as a function of excitation energy. Thus, Stiopkin et al.[37] demonstrate how 2D spectroscopy differentiates between population relaxation and exchange narrowing in room-temperature J-aggregates.

J-aggregates are long linear chains of identical molecules that self-assemble due to electrostatic interactions.[3,5] Strong intermolecular coupling in J-aggregates leads to highly delocalized excitons, each with a delocalization length, L_{DEL}, spanning tens of monomers.[5,8] Spectra of J-aggregates display exchange narrowing:[38] the line width of an exciton transition peak is significantly reduced because both static disorder and dynamic (random energy) fluctuations at different monomer sites average out over the exciton wave function's spatial extent.

Stiopkin et al. consider the exciton energy dependence of the antidiagonal peak width evolution in absolute value 2D spectra of BIC J-aggregates (Figure 5a).[37] As in LH3, the excitons are not individually resolved; however the band's antidiagonal width (ADW) is visibly nonuniform in energy. Figure 5b shows that the ADW is lowest for intermediate exciton energies in the band at all waiting times T.

Energy-dependent dynamics can be explained by a model that includes both exchange narrowing and population relaxation to reproduce the experimentally observed frequency-dependent line widths, as shown in Figure 5c. Population
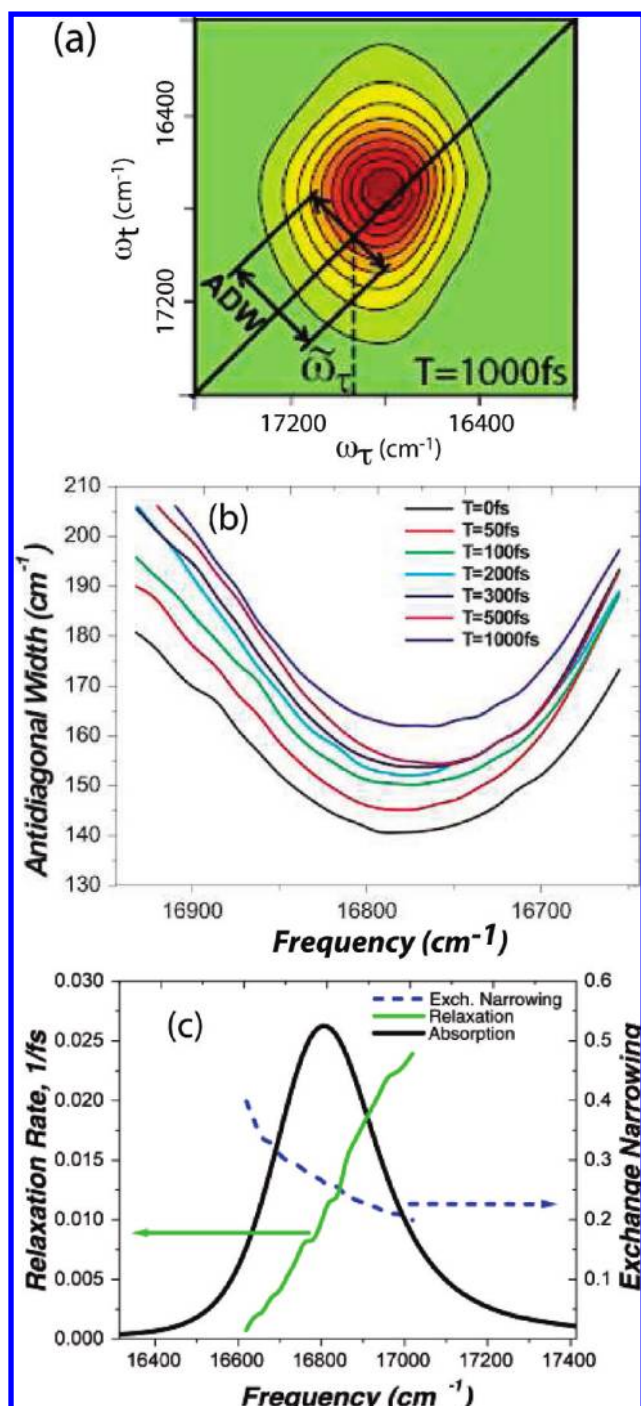
FIGURE 5. Discerning population relaxation and exchange narrowing in BIC J-aggregates:[37] (a) absolute value 2D spectrum of the J-aggregate exciton band; (b) exciton band ADW energy-dependent evolution; (c) simulated energy dependence of population relaxation and exchange narrowing.

relaxation within the exciton band is more probable from higher states than lower ones since higher states have more attainable relaxation channels. Thus, lifetime broadening preferentially increases the ADW at the top of the band. In contrast, the exciton delocalization length is larger for higher energy states (Figure 5c), resulting in more exchange narrow-

ing and a narrower ADW at higher energies. The interplay between these two mechanisms results in the "U"-shaped frequency-dependent ADW in Figure 5b.

In addition to explaining the observed dynamics, these findings enable an estimate of the delocalization length and refinements in the modeling of electron–phonon coupling. In sum, multiple critical aggregate characteristics may be determined from the combination of 2D spectroscopy's resolution of homogeneous line widths and spectral resolution of excitation and emission energies.[37,39]

3.4. Electronic Coherence and Energy Landscape Determination. Thus far, the Liouville pathways explicitly discussed had population density matrix elements during the waiting time. It is also possible to obtain an excitonic coherence $|e_i\rangle\langle e_j|$ during this period, in which superposition states between excitons exist within individual aggregates. The time evolution of the coherence $|e_i\rangle\langle e_j|$ during the waiting time has an oscillating phase factor $e^{-i\omega_{ij}T}$, resulting in quantum beats in the 2D spectra. This is a powerful aspect of the technique because it exploits a true quantum effect in the phase evolution of the optical polarization and can be related quantitatively to coherence dynamics in the system.[28,40,42,43]

Recently, 2D spectra of FMO were measured in order to observe such behavior.[41] Prominent amplitude oscillations were observed and quantified by considering the evolution of the diagonal cut of the spectrum (Figure 6a) as a function of waiting time (Figure 6b). Remarkably, the peak oscillation persisted throughout the 660 fs extent of the measurements.

Multiple signatures corroborate that electronic coherence is responsible for the observed oscillations. First, the beat spectrum of the amplitude oscillations of the spectrally isolated lowest-energy exciton peak (Figure 6c) is consistent with a prediction based on the FMO Hamiltonian.[31,41] Second, as expected,[42] the peak's aspect ratio oscillations are anticorrelated to its amplitude oscillations (Figure 6d), in agreement with theory.[28] These techniques are not limited to the study of photosynthetic complexes and have recently been employed to examine long-lived coherent energy transport in conjugated polymers.[44]

To propose a hypothesis for the surprising persistence of exciton superpositions, consider a photon echo study performed on a coupled dimer of pigments in a bacterial reaction center.[45] The experimental results of the study were successfully modeled only when assuming that the surrounding protein fluctuations at the different pigment sites were correlated. These correlations reduce the fluctuations of the energy gap between the two related exciton states, enabling their long-lasting coherence. Such correlated protein motions
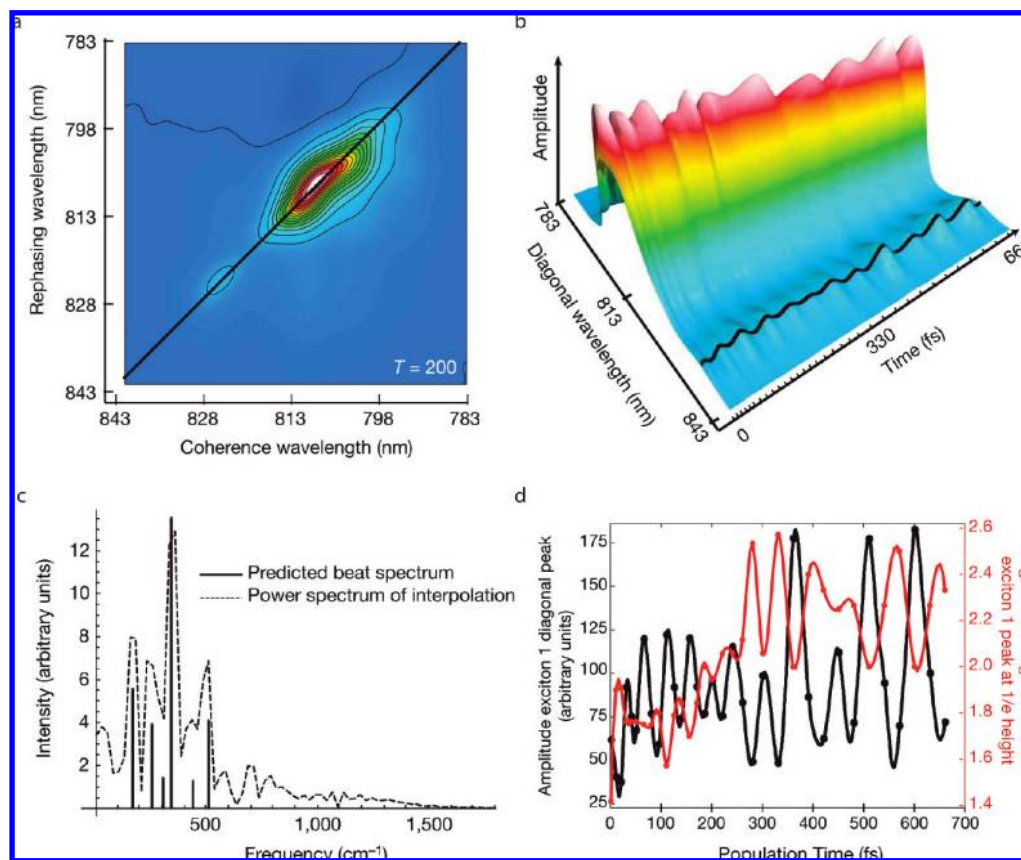
FIGURE 6. Electronic quantum coherence in the FMO complex:[41] (a) the T = 200 fs 2D spectrum of isolated FMO complexes at 77 K; (b) diagonal cuts of FMO 2D spectra plotted versus waiting time—the amplitude beating of the lowest exciton peak is traced by a solid black line; (c) the Fourier transform of the oscillating black trace in panel b (dashed curve) agrees with a beat spectrum predicted by the excitonic energy structure of FMO (black sticks); (d) the amplitude of the exciton 1 diagonal peak (black curve) from panel b and the ratio of the diagonal to antidiagonal widths of the peak (red curve).

were posited to arise since both pigments contributing to the two excitons were situated along the same α-helix.[46] A similar phenomenon could explain the long-lived quantum beats observed in FMO. Such a manifestation should improve the efficiency for excitation energy transfer by allowing reversible sampling of the energy landscape, avoiding energy trapping in local minima, and enabling the correct energy sink to effectively extract excitation energy when being sampled over the course of the oscillations.[47,48]

The analysis used to study excitonic quantum coherence in FMO can be adapted to determine the transition energies of the excitons. Though the experimental power spectrum (Figure 6c) is shown to agree with a preestablished model, if a model were less certain, the experimental data could be used to refine it. Indeed, instead of considering the power spectrum at a single exciton energy, as done here, the entire data set plotted in Figure 6b can be Fourier transformed with respect to waiting time to obtain the complete exciton land-

scape.[30] Such a technique should very efficiently pinpoint transition energies compared with traditional modeling strategies.

3.5. Spatial Structure Determination of Molecular Aggregates. The following two examples show how 2D electronic spectroscopy can also provide structural information. Though structures for pigment–protein complexes such as FMO are well characterized, there are many cases in which atomic-resolution structures for molecular complexes remain elusive. Knowledge of the precise chromophore configurations within such complexes is important because it forms the basis for models of the resulting excitation energy dynamics.[2,7,9]

3.5.1. Proposing Pigment Arrangement in LH4. Like LH3, light-harvesting complex 4 (LH4) is a light-harvesting variant expressed by photosynthetic purple bacteria in low light conditions.[49] Unlike LH3, LH4 has a single band in its spectrum at 800 nm and has a total of 32 BChl molecules dis-
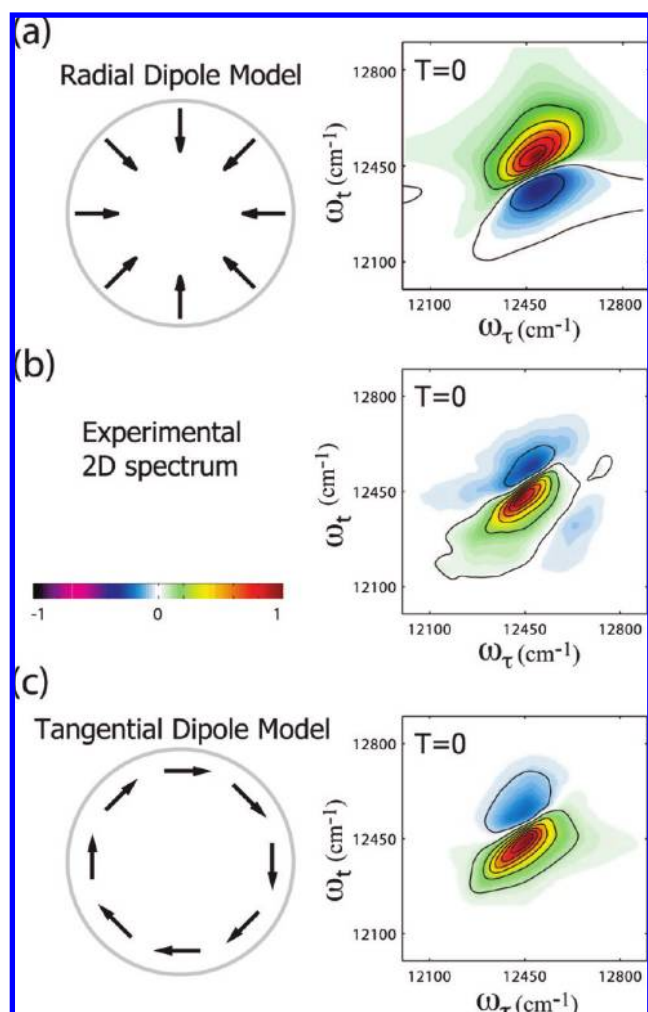
FIGURE 7. Spectral sensitivity to chromophore configuration in LH4.[25] Radial (a) and tangential (c) dipole models for relevant chromophores in LH4 are compared with the experimentally obtained $T = 0$ spectrum (b).

tributed among 8 identical protein subunits in the ring-like structure.[25] It is suspected that LH4 is significantly different in structure from other bacterial light-harvesting complexes, and a model of the structure has been proposed by mapping its electron density at 7.5 Å resolution.[50] This model assumes that the dipole moments of some of the BChls are oriented radially, like the spokes of a wheel (Figure 7a); however there is no high-resolution crystal structure to confirm this. Recently, 2D electronic spectroscopy was used to assess the validity of this model;[25] the results (Figure 7b) indicate that these BChls are unlikely to be radially oriented and must instead be angled nearly parallel to one another, tracing out the tangents of a circle, as shown in Figure 7c.

Recall that in the study of LH3 in section 3.2, the asymmetry of negative peaks in the 2D spectra was a sensitive indicator of electronic coupling, which depends on the proximity and relative orientation of adjacent dipoles. For LH4,

the location of similarly generated negative features establishes the orientation of the relevant BChls. In Figure 7, an experimentally obtained spectrum is compared with numerically generated ones. As can be seen, the position of the negative peaks in the tangential dipole model match the experimental data, while those in the radial model do not. In essence, the nature of electronic coupling to which 2D spectroscopy is highly sensitive has forced a structural model with several angstrom resolution to be reconsidered.

3.5.2. Structural Information from 2D Polarization Techniques. The features in spectra presented thus far generally contain multiple overlapping peaks. Here, we show how laser pulse polarization can be used to enhance or suppress the signal from different Liouville pathways that comprise a congested feature.[51,52] Each Liouville pathway is associated with a unique dipole-angle-dependent orientational factor that is a function of the field polarizations used in the pulse sequence. Therefore, by correlating an isolated peak with a particular pathway, its pulse polarization-dependent signal strength provides structural information: the angle between the exciton dipoles involved can be determined.[53]

Orientational factors for isotropic ensembles are the orientationally averaged products of the projection of each of the four transition dipole vectors $\vec{\mu}_i$ involved in the pathway with its corresponding laser pulse polarization vector: $\langle(\vec{\mu}_4 \cdot \hat{\varepsilon}_4)(\vec{\mu}_3 \cdot \hat{\varepsilon}_3)(\vec{\mu}_2 \cdot \hat{\varepsilon}_2)(\vec{\mu}_1 \cdot \hat{\varepsilon}_1)\rangle$. Clearly, the corresponding signal strength of such factors depends on the polarization of laser pulses $\hat{\varepsilon}_i$.[51,52] Various polarization sequences of the form $\langle\theta_1,\theta_2,\theta_3,\theta_{LO}\rangle$, where θ_i is the linear polarization angle of pulse i, have been used in 2D IR spectroscopy[54] and extended to the visible to effectively parse 2D electronic spectra. For example, using the $\langle+60°,-60°,0,0\rangle$ sequence in the electronic regime demonstrated the suppression of FMO diagonal peaks, enabling a closer look at the remaining, often overpowered, cross-peaks.[55]

In order to determine aggregate structure, Read et al.[24] studied the exciton $4 \rightarrow 2$ population transfer cross-peak in FMO spectra. The absolute value of the nonrephasing 2D spectrum taken at $T = 400$ fs was considered for polarization sequences $\langle+45°,-45°,0,0\rangle$ and $\langle+75°,-75°,0,0\rangle$ (Figure 8a). The peak (white arrow) is distinctly visible in the $\langle+75°,-75°,0,0\rangle$ spectrum, but noticeably less prominent in the $\langle+45°,-45°,0,0\rangle$ spectrum. The orientational factors for these polarization sequences as a function of the projection angle between the dipoles of the two involved excitonic states are plotted in Figure 8b. The polarization sequence-dependent signal amplitude variation observed in the experiment is
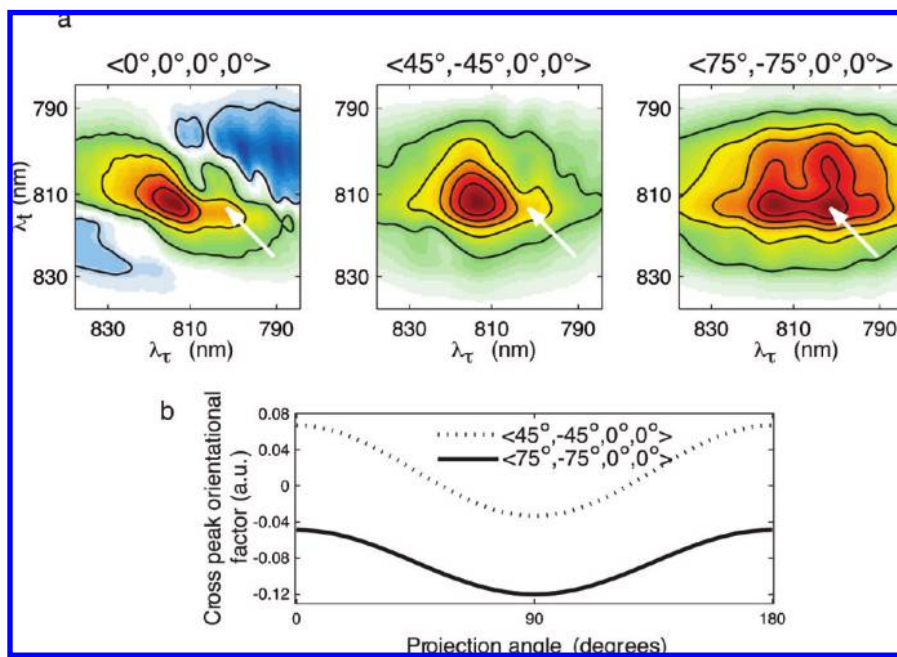
FIGURE 8. Determining dipole angles in FMO using polarization-based 2D spectroscopy:[24] (a) $\langle 0,0,0,0 \rangle$, $\langle +45°,-45°,0,0 \rangle$ and $\langle +75°,-75°,0,0 \rangle$ experimental $T = 400$ fs absolute value nonrephasing spectra—arrows indicate the exciton $4 \rightarrow 2$ cross-peak; (b) orientational factors for the polarization sequences employed.

only reproduced by a dimer system simulation if the angle between the two dipoles is set to ~40°. This agrees with the well-characterized model for FMO that predicts $\phi = 38°$ between exciton dipoles 2 and 4.[32]

The above example shows that 2D electronic spectroscopy, combined with theoretical modeling, is capable of obtaining structural information about molecular aggregates. Similar strategies could be implemented for systems less well-characterized than FMO. Since the study of these systems cannot rely as heavily on simulations, it will be essential to obtain more quantitative information directly from experimental data. In this vein, note that all possible polarization sequences can be constructed from linear combinations of three orthogonal sequences: $\{\langle 90°,90°,0,0 \rangle, \langle 90°,0,90°,0 \rangle, \langle 0,90°,90°,0 \rangle\}$.[51] Therefore, it should in principle be possible to construct arbitrary linear combinations of polarization-dependent *spectra* taken with these three polarization conditions in order to enhance or suppress many different contributions[56] and to obtain a host of structural information.

4. Outlook

Much of the power of 2D spectroscopy lies in the ability to resolve multiple transitions and processes in parallel, and continued refinements to the technique, such as those described above, will continue to enhance its acuity. The consequences of these explorations will no doubt improve our understanding of naturally occurring as well as artificial electronically coupled systems and will drive the development of novel, robust synthetic structures with similar functional objectives.

BIOGRAPHICAL INFORMATION

Naomi S. Ginsberg (Ph.D. Physics, 2007, Harvard University) is a Seaborg Postdoctoral Fellow in Physical Biosciences at LBNL. Light–matter interactions link her research interests in novel probes of photosynthetic complexes and of Bose-condensed atomic gases and ultraslow light.

Yuan-Chung Cheng (Ph.D. Theoretical Chemistry, 2006, MIT) was formerly a postdoctoral fellow at UC Berkeley where he focused on theoretical studies of excitation energy transfer in molecular aggregates and nonlinear optical spectroscopic techniques. He is currently an assistant professor at National Taiwan University, Taipei, Taiwan.

Graham R. Fleming (Ph.D. Physical Chemistry, 1974, University of London) is Melvin Calvin Distinguished Professor of Chemistry and Vice Chancellor for Research at UC Berkeley. His

research group studies ultrafast chemical and biological dynamics in the condensed phase.

REFERENCES

1 van Amerongen, H.; Valkunas, L.; van Grondelle, R. *Photosynthetic Excitons*; World Scientific Publishing Company: Singapore, 2000.

2 Blankenship, R. E. *Molecular Mechanisms of Photosynthesis*; Blackwell Science: Oxford, U.K., 2002.

3 Mishra, A.; Behera, R.; Behera, P.; Mishra, B.; Behera, G. Cyanines during the 1990s: A review. *Chem. Rev.* **2000**, *100*, 1973–2011.

4 Gust, D.; Moore, T. A.; Moore, A. L. Mimicking photosynthetic solar energy transduction. *Acc. Chem. Res.* **2001**, *34*, 40–48.

5 Kobayashi, T. *J-Aggregates*; World Scientific: Singapore, 1996.

6 Hu, X.; Ritz, T.; Damjanovic, A.; Autenrieth, F.; Schulten, K. Photosynthetic apparatus of purple bacteria. *Q. Rev. Biophys.* **2002**, *35*, 1–62.

7 Scholes, G. D.; Fleming, G. R. Energy transfer and photosynthetic light harvesting. *Adv. Chem. Phys.* **2005**, *132*, 57–130.

8 Spano, F. C. Excitons in conjugated oligomer aggregates, films, and crystals. *Annu. Rev. Phys. Chem.* **2006**, *57*, 217–243.

9 Cheng, Y.-C.; Fleming, G. R. Dynamics of light harvesting in photosynthesis. *Annu. Rev. Phys. Chem.* **2008**, *60*, 241–262.

10 Mukamel, S. Multidimensional femtosecond correlation spectroscopies of electronic and vibrational excitations. *Annu. Rev. Phys. Chem.* **2000**, *51*, 691–729.

11 Jonas, D. M. Two-dimensional femtosecond spectroscopy. *Annu. Rev. Phys. Chem.* **2003**, *54*, 425–463.

12 Cho, M.; Brixner, T.; Stiopkin, I. V.; Vaswani, H. M.; Fleming, G. R. Two dimensional electronic spectroscopy of molecular complexes. *J. Chin. Chem. Soc.* **2006**, *53*, 15–24.

13 Cho, M. Coherent two-dimensional optical spectroscopy. *Chem. Rev.* **2008**, *108*, 1331–1418.

14 Ernst, R. R.; Bodenhausen, G.; Wokaun, A. *Principles of Nuclear Magnetic Resonance in One and Two Dimensions*; Oxford University Press: Oxford, U.K., 1990.

15 Hamm, P.; Lim, M.; Hochstrasser, R. M. Structure of the amide I band of peptides measured by femtosecond nonlinear-infrared spectroscopy. *J. Phys. Chem. B* **1998**, *102*, 6123–6138.

16 Ganim, Z.; Chung, H. S.; Smith, A. W.; DeFlores, L. P.; Jones, K. C.; Tokmakoff, A. Amide I two-dimensional infrared spectroscopy of proteins. *Acc. Chem. Res.* **2008**, *41*, 432–441.

17 Lepetit, L.; Cheriaux, G.; Joffre, M. Linear techniques of phase measurement by femtosecond spectral interferometry for applications in spectroscopy. *J. Opt. Soc. Am. B* **1995**, *12*, 2467–2474.

18 Ogilvie, J. P.; Cowan, M. L.; Miller, R. J. D. Diffractive optics-based heterodyne detected three-pulse photon echo. In *Ultrafast Phenomena XIII*; Miller, R. J. D.; Murnane, M. M.; Scherer, N. F.; Weiner, A. M., Eds.; Springer-Verlag: Berlin, 2003; pp. 571–573.

19 Brixner, T.; Stiopkin, I. V.; Fleming, G. R. Tunable two-dimensional femtosecond spectroscopy. *Opt. Lett.* **2004**, *29*, 884–886.

20 Mukamel, S. *Principles of Nonlinear Optical Spectroscopy*; Oxford University Press: Oxford, U.K., 1995.

21 Hybl, J.; Ferro, A. A.; Jonas, D. M. Two-dimensional fourier transform electronic spectroscopy. *J. Chem. Phys.* **2001**, *115*, 6606–6622.

22 This is fundamentally different from analogous magnetic resonance experiments in which pulses induce significant changes to the population of nuclear spin states.

23 Brixner, T.; Stenger, J.; Vaswani, H. M.; Cho, M.; Blankenship, R. E.; Fleming, G. R. Two-dimensional spectroscopy of electronic couplings in photosynthesis. *Nature* **2005**, *434*, 625–628.

24 Read, E. L.; Schlau-Cohen, G. S.; Engel, G. S.; Wen, J.; Blankenship, R. E.; Fleming, G. R. Visualization of excitonic structure in the Fenna-Matthews-Olson photosynthetic complex by polarization-dependent two-dimensional electronic spectroscopy. *Biophys. J.* **2008**, *95*, 847–856.

25 Read, E. L.; Schlau-Cohen, G. S.; Engel, G. S.; Georgiou, T.; Papiz, M. Z.; Fleming, G. R. Pigment organization and energy level structure in light-harvesting complex 4: Insights from two-dimensional electronic spectroscopy. *J. Phys. Chem. B* **2009**, *113*, 6495–6504.

26 Ge, N. H.; Zanni, M. T.; Hochstrasser, R. M. Effects of vibrational frequency correlations on two-dimensional infrared spectra. *J. Phys. Chem. A* **2002**, *106*, 962–972.

27 Khalil, M.; Demirdoven, N.; Tokmakoff, A. Coherent 2D IR spectroscopy: Molecular structure and dynamics in solution. *J. Phys. Chem. A* **2003**, *107*, 5258–5279.

28 Cheng, Y.-C.; Fleming, G. R. Coherence quantum beats in two-dimensional electronic spectroscopy. *J. Phys. Chem. A* **2008**, *112*, 4254–4260.

29 Roberts, S. T.; Loparo, J. J.; Tokmakoff, A. Characterization of spectral diffusion from two-dimensional line shapes. *J. Chem. Phys.* **2006**, *125*, 084502.

30 Calhoun, T. R.; Ginsberg, N. S.; Schlau-Cohen, G. S.; Cheng, Y.-C.; Ballottari, M.; Bassi, R.; Fleming, G. R. Observation of quantum coherence in photosynthetic complexes by two-dimensional electronic spectroscopy. In *Ultrafast Phenomena XVI*; Corkum, P. B.; Nelson, K. A.; Riedle, E.; Schoenlein, R. W.; De Silvestri, S., Eds.; Springer-Verlag: Berlin, in press.

31 Cho, M.; Vaswani, H. M.; Brixner, T.; Stenger, J.; Fleming, G. R. Exciton analysis in 2D electronic spectroscopy. *J. Phys. Chem. B* **2005**, *109*, 10542–10556.

32 Adolphs, J.; Renger, T. How proteins trigger excitation energy transfer in the FMO complex of green sulfur bacteria. *Biophys. J.* **2006**, *91*, 2778–2797.

33 Wen, J.; Zhang, H.; Gross, M. L.; Blankenship, R. E. Membrane orientation of the FMO antenna protein from Chlorobaculum tepidum as determined by mass spectrometry-based footprinting. *Proc. Natl. Acad. Sci. U.S.A.* **2009**, *106*, 6134–6139.

34 Zigmantas, D.; Read, E. L.; Mancal, T.; Brixner, T.; Gardiner, A. T.; Cogdell, R. J.; Fleming, G. R. Two-dimensional electronic spectroscopy of the B800-B820 light-harvesting complex. *Proc. Natl. Acad. Sci. U.S.A.* **2006**, *103*, 12672–12677.

35 Cheng, Y.-C.; Silbey, R. J. Coherence in the B800 ring of purple bacteria LH2. *Phys. Rev. Lett.* **2006**, *96*, 028103.

36 Fidder, H.; Knoester, J.; Wiersma, D. A. Superradiant emission and optical dephasing in J-aggregates. *Chem. Phys. Lett.* **1990**, *171*, 529–536.

37 Stiopkin, I. V.; Brixner, T.; Yang, M.; Fleming, G. R. Heterogeneous exciton dynamics revealed by two-dimensional optical spectroscopy. *J. Phys. Chem. B* **2006**, *110*, 20032–20037.

38 Knapp, E. W. Lineshapes of molecular aggregates, exchange narrowing and intersite correlation. *Chem. Phys.* **1984**, *85*, 73–82.

39 Dijkstra, A. G.; la Cour Jansen, T.; Knoester, J. Localization and coherent dynamics of excitons in the two-dimensional optical spectrum of molecular J-aggregates. *J. Chem. Phys.* **2008**, *128*, 164511.

40 Note that intercomplex coherence should not be confused with electronic coherence between the excitons *within* an individual complex. While electronic coherence results from quantum superpositions of electronic states in a given complex, intercomplex coherence is a result of classically coherent laser light initiating the dynamics of multiple redundant complexes simultaneously.

41 Engel, G. S.; Calhoun, T. R.; Read, E. L.; Ahn, T.-K.; Mancal, T.; Cheng, Y.-C.; Blankenship, R. E.; Fleming, G. R. Evidence for wavelike energy transfer through quantum coherence in photosynthetic systems. *Nature* **2007**, *446*, 782–786.

42 Pisliakov, A. V.; Mancal, T.; Fleming, G. R. Two-dimensional optical three-pulse photon echo spectroscopy. II. Signatures of coherent electronic motion and exciton population transfer in dimer two-dimensional spectra. *J. Chem. Phys.* **2006**, *124*, 234505.

43 Cheng, Y.-C.; Engel, G. S.; Fleming, G. R. Elucidation of population and coherence dynamics using cross-peaks in two-dimensional electronic spectroscopy. *Chem. Phys.* **2007**, *341*, 285–295.

44 Collini, E.; Scholes, G. D. Coherent intrachain energy migration in a conjugated polymer at room temperature. *Science* **2009**, *323*, 369–373.

45 Lee, H.; Cheng, Y.-C.; Fleming, G. R. Coherence dynamics in photosynthesis: Protein protection of excitonic coherence. *Science* **2007**, *316*, 1462–1465.

46 Müh, F.; Madjet, M. E.-A.; Adolphs, J.; Abdurahman, A.; Rabenstein, B.; Ishikita, H.; Knapp, E.-W.; Renger, T. α-Helices direct excitation energy flow in the Fenna Matthews Olson protein. *Proc. Natl. Acad. Sci. U.S.A.* **2007**, *104*, 16862–16867.

47 Mohseni, M.; Rebentrost, P.; Lloyd, S.; Aspuru-Guzik, A. Environment-assisted quantum walks in photosynthetic energy transfer. *J. Chem. Phys.* **2008**, *129*, 174106.

48 Ishizaki, A.; Fleming, G. R. Unified treatment of quantum coherent and incoherent hopping dynamics in electronic energy transfer: Reduced hierarchy equation approach. *J. Chem. Phys.* **2009**, *130*, 234111.

49 Scheuring, S.; Goncalves, R. P.; Prima, V.; Sturgis, J. N. Mimicking photosynthetic solar energy transduction. *J. Mol. Biol.* **2006**, *358*, 83–96.

50 Hartigan, N.; Tharia, H.; Sweeney, F.; Lawless, A.; Papiz, M. The 7.5-Å electron density and spectroscopic properties of a novel low-light B800 LH2 from *Rhodopseudomonas palustris*. *Biophys. J.* **2002**, *82*, 963–977.

51 Hochstrasser, R. M. Two-dimensional IR-spectroscopy: Polarization anisotropy effects. *Chem. Phys.* **2001**, *266*, 273–284.

52 Dreyer, J.; Moran, A. M.; Mukamel, S. Tensor components in three pulse vibrational echoes of a rigid dipeptide. *Bull. Korean Chem. Soc.* **2003**, *24*, 1091–1096.

53 Cho, M.; Fleming, G. R. The integrated photon echo and solvation dynamics. II peak shifts and two-dimensional photon echo of a coupled chromophore system. *J. Chem. Phys.* **2005**, *123*, 114506.

54 Zanni, M. T.; Ge, N. H.; Kim, Y. S.; Hochstrasser, R. M. Two-dimensional IR spectroscopy can be designed to eliminate the diagonal peaks and expose only the cross-peaks needed for structure determination. *Proc. Natl. Acad. Sci. U.S.A.* **2001**, *98*, 11265–11270.

55 Read, E. L.; Engel, G. S.; Calhoun, T. R.; Mancal, T.; Ahn, T.-K.; Blankenship, R. E.; Fleming, G. R. Cross-peak-specific two-dimensional electronic spectroscopy. *Proc. Natl. Acad. Sci. U.S.A.* **2007**, *104*, 14203–14208.

56 Abramavicius, D.; Voronine, D. V.; Mukamel, S. Unravelling coherent dynamics and energy dissipation in photosynthetic complexes by 2D spectroscopy. *Biophys. J.* **2008**, *94*, 3613–3619.